ENGINEERING Biomass
https://doi.org/10.2738/ENGB.2026.0003

Original Research

Boosting Functional Performance of Soy Protein Isolate via Controlled Deamidation: Insights into Structure-function Relationships

Shangwen Chen[1], Yawen Huang[1,2], Fazhan Zhong[1], Dengfeng Peng[1], Yashu Chen[1], Bin Zhou[2], Zisong Li[3], Qianchun Deng (✉)[1], Ziyu Deng (✉)[1]

1 Key Laboratory of Oilseeds Processing, Ministry of Agriculture, Oil Crops Research Institute, Chinese Academy of Agricultural Sciences, Wuhan 430062, China
2 School of Life and Health Sciences, Hubei University of Technology, Wuhan 430068, China
3 Shandong Xingquan Oil Products Co., Ltd., Linyi 371327, China

© The Author(s) 2026. This article is published by Higher Education Press.

GRAPHICAL ABSTRACT

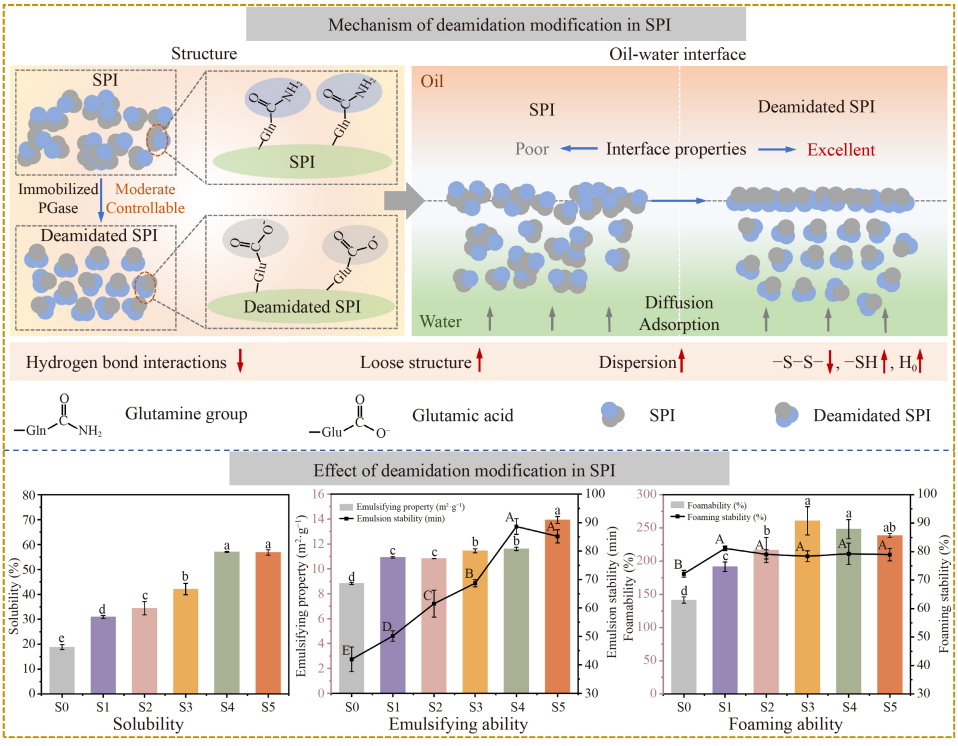

HIGHLIGHTS

- Optimized process yields high deamidation with minimal hydrolysis of SPI via RSM.
- The solubility, emulsifiability, and foaming properties of SPI were greatly enhanced.
- Controllable and mild deamidation significantly improved the flavor of SPI.
- Mild enzymatic process optimally tailored SPI structure for superior functionality.
- Deamidation degree-structure-function relationship of SPI was elucidated.

Received 15 Apr 2026; accepted 22 May 2026

E-mails: dengqianchun@caas.cn (Deng Q.),
dengziyu@caas.cn (Deng Z.).

ABSTRACT The functional properties of soy protein isolate (SPI) can be enhanced through deamidation. However, the relationships among deamidation degree, structural changes, and functionality remain insufficiently understood. In this study, immobilized protein glutaminase (PGase) was used to achieve mild, controllable SPI deamidation. Response surface methodology was applied to optimize reaction conditions, maximizing deamidation while minimizing hydrolysis. The optimal parameters—54.93 °C, pH 6.80, and an enzyme-to-substrate ratio of 26.65 $U \cdot g^{-1}$—yielded SPI with high deamidation and low hydrolysis. Increasing deamidation initially improved SPI functionality, but it then plateaued. At the optimal deamination level, the solubility, emulsifying activity, and foaming capacity of SPI increased by approximately 200%, 60%, and 85%, respectively. Additionally, umami and saltiness perceptions were enhanced, while bitterness was significantly reduced. Structural changes were assessed using SDS-PAGE, particle size analysis, zeta potential measurements, microscopy, and spectral analysis. The modification mechanism was further investigated by analyzing oil–water interfacial properties. These findings clarify the influence of deamidation degree on SPI structure and functionality, offering insights for food industry applications.

KEYWORDS Soy protein isolate; Immobilized protein glutaminase; Deamidation; Functional properties enhancement; Structure-function relationship

1 Introduction

Plant proteins have received considerable research attention in recent years because of their documented health benefits and nutritional value [1–3]. Soy protein isolate (SPI), extracted and purified from defatted soybean meal, provides all essential amino acids and is especially rich in lysine. Therefore, SPI serves as a valuable complement to cereal-based diets and acts as a nutritionally complete protein source [1,4]. SPI also exhibits protein digestibility comparable to that of animal proteins, highlighting its potential to support human health [1,5]. However, the high glutamine content in SPI can promote protein aggregation or precipitation through hydrogen bonding, hydrophobic interactions, and network formation, which often leads to poor solubility [6,7]. The low solubility of SPI further impairs other functional properties, such as emulsification, foaming, and gelation. These limitations restrict the application of SPI in the food industry, particularly as a functional ingredient. As a result, improving the industrial suitability of SPI has become a central research focus. Current strategies to enhance SPI solubility encompass physical, chemical, and enzymatic approaches [8]. Physical methods alter protein structure to facilitate dispersion in aqueous systems. For example, ultrasonic treatment loosens protein conformation [9], while high-pressure homogenization reduces particle size and increases surface area [10]. These techniques, however, often require specialized equipment [8]. Chemical methods modify amino acid side chains to change surface charge and hydrophilicity, such as through pH adjustment [11] or phosphorylation [12], but these processes are generally not environmentally sustainable. Enzymatic methods use proteases to cleave proteins into smaller peptides, thereby exposing additional polar groups. Nevertheless, this approach may compromise native protein properties and introduce safety concerns [13,14].

Deamidation refers to the conversion of protein amide groups into carboxyl groups through physical, chemical, or enzymatic mechanisms. This modification increases the negative charge of proteins and enhances electrostatic repulsion, resulting in a more extended protein structure, weakened hydrogen bonds, reduced hydrophobic interactions, and ultimately improved protein solubility [15]. Physical methods such as high temperature or pressure [16], and chemical approaches such as pH adjustment [17], generally lack site-specificity and may present safety concerns. In contrast, enzymatic deamidation effectively addresses these limitations [18,19]. However, L-glutaminase is effective exclusively on free glutamine and does not modify large protein molecules [20]. Transglutaminase catalyzes protein cross-linking [21]. Certain proteases may indirectly promote deamidation via non-specific hydrolysis, which frequently results in the formation of by-products [18]. Protein glutaminase (PGase) offers significant advantages because of its high specificity for glutamine residues in protein side chains and its lack of protein hydrolysis activity [22,23]. PGase treatment has been shown to increase the solubility of rice [16] and wheat [24] proteins by up to 100%. Nevertheless, increased deamidation does not consistently result in improved functional properties [25]. The relationship among the degree of deamidation, molecular structure, and protein functionality remains insufficiently understood, highlighting the necessity for precise control of deamidation to clarify these interactions.

In preliminary studies, PGase was immobilized on a composite gel carrier formed by cross-linking sunflower pollen microgel (SPMG) with sodium alginate and Ca^{2+}. Reaction conditions, including temperature, pH, and enzyme-to-substrate ratio, were optimized to produce SPI with controlled degrees of deamidation. The functional and flavor properties of these SPI samples were subsequently evaluated. Additionally, the relationship

between deamidation degree, molecular structure, and functional performance was examined using molecular, sensory, spectroscopic, and interfacial analyses. This approach provides a novel strategy for enhancing the application of SPI in the food industry.

2 Materials and Methods

2.1 Materials

Sunflower pollen was provided by Belle Bee Biotechnology Co., Ltd. (Shanghai, China). PGase was purchased from Amano Enzyme Preparation Co., Ltd. (Japan). Soy protein isolate (SPI, > 85%) was purchased from Huayi Biotechnology Co., Ltd. (Shandong, China). β-mercaptoethanol and 8-aminonaphthalene-1-sulfonic acid were purchased from the Sigma-Aldrich (America). The BCA protein concentration determination kit was acquired from Labgic Technology Co., Ltd. (Anhui, China). Disodium hydrogen phosphate, dipotassium hydrogen phosphate, urea, and ethylenediaminetetraacetic acid and all other reagents were acquired from Sinopharm Group Chemical Reagent Co., Ltd. (Shanghai, China). Millipore water was used for all experiments.

2.2 Preparation of PGase immobilized on composite gel carriers

SPMG was prepared from sunflower pollen through three sequential steps: defatting, removal of cytoplasmic contents, and microgel formation [26]. Subsequently, SPMG was thoroughly mixed with a sodium alginate solution (3%, w/v) at a 2:1 volume ratio and then dripped into a $CaCl_2$ solution (2%, w/v). Following a reaction period of two hours, the mixture was subjected to a series of rinses, repeated two to three times, to yield the composite gel carrier. Subsequently, 1-ethyl-(3-dimethylaminopropyl)-carbodiimide (EDC, 0.1%, w/v) and N-hydroxybutyrylimidazole (NHS, 0.1%, w/v) are to be added in a 1:1 volume ratio. The mixture was subsequently amalgamated with the composite gel carrier at a volumetric ratio of 3 mL:1 g. After a 1-hour reaction period, the carrier surface was thoroughly washed. Finally, the composite gel carrier was mixed with the PGase solution [1%, w/v, prepared in 0.02 $mol \cdot L^{-1}$ phosphate buffered saline (PBS) buffer at pH 6.5] at a ratio of 1 g:4 mL. The mixture was heated to 25 °C and rotated at 150 rpm for 3 hours, including a 0.5-hour vacuum treatment. Subsequently, residual PGase on the carrier surface was washed off, yielding a composite gel carrier immobilized with PGase (carrier enzyme activity approximately 40 $U \cdot g^{-1}$).

2.3 Optimization of conditions for immobilized PGase-modified SPI

2.3.1 Single-factor experiment

A solution of SPI at 10 $mg \cdot mL^{-1}$ was prepared. Utilizing the higher deamidation degree and lower hydrolysis degree of SPI as evaluation criteria, the objective was to optimize the conditions for immobilized PGase-modified SPI by varying the reaction temperature (30–60 °C), the reaction pH (4–8), and the enzyme-to-substrate ratio (E/S, 13.0–55.5 $U \cdot g^{-1}$).

2.3.2 Response surface experiment

Following the single-factor experiments described in Section 2.3.1, the effects of reaction temperature (A: 50, 55, 60 °C), pH (B: 6, 7, 8), and E/S ratio (C: 13, 21.5, 30 $U \cdot g^{-1}$) on the degrees of deamidation and hydrolysis of SPI were systematically evaluated. A three-factor, three-level Box-Behnken design was employed to develop regression models and determine the optimal conditions for maximizing deamidation while minimizing hydrolysis.

2.4 Preparation and characterization of modified SPI

2.4.1 Preparation of modified SPI

Under the optimized conditions described in Section 2.3.2, a 1% SPI solution was prepared and combined with immobilized PGase. The deamidation degree of SPI was determined at 0, 15, 45, 75, 90, 120, and 180 minutes, resulting in values of 0%, 33.43%, 39.46%, 47.40%, 48.82%, and 47.61%, respectively. Upon completion of the reaction, immobilized PGase was removed, and the samples were freeze-dried to produce SPI powders with distinct deamidation degrees. These powders were designated as S0, S1, S2, S3, S4, and S5 for subsequent analysis.

2.4.2 Determination of functional characteristics and aggregation properties of modified SPI

2.4.2.1 Subunit composition determination

A 1.5 $mg \cdot mL^{-1}$ SPI sample solution was prepared. Subunit band analysis was subsequently performed using an electrophoresis system (Mini-Protean-3, Bio-Rad, USA). A standard molecular weight marker (~250 kDa) was run in parallel with the samples [27].

2.4.2.2 Determination of solubility

SPI samples were dissolved in PBS buffer (0.02 mol·L^{-1}, pH 7.0) to prepare 1 mg·mL^{-1} solutions and subsequently centrifuged at 12,000 rpm for 5 minutes. Protein content in the supernatant was quantified using a BCA protein assay kit. Solubility was expressed as the percentage of supernatant protein relative to the total protein content [28].

2.4.2.3 Determination of emulsifying properties

A sample solution (10 mg·mL^{-1}) was combined with perilla oil at a 3:1 (v/v) ratio and homogenized at 12,000 rpm for 2 minutes using a high-speed shear homogenizer (T25, IKA, Germany). The resulting emulsion was subsequently diluted 100-fold with 0.1% (w/v) SDS solution. Absorbance at 500 nm was determined against a 0.1% SDS blank using a spectrophotometer [ultraviolet (UV)−1900, Shimadzu Co., Japan]. Emulsifying activity (EAI) and emulsion stability (ESI) were calculated using the following equations [29].

$$\mathrm{EAI}\ (\mathrm{m}^2\cdot\mathrm{g}^{-1}) = 2 \times 2.303 \times A_0 \times N/(10{,}000 \times k \times L \times C) \quad (1)$$

$$\mathrm{ESI}\ (\mathrm{min}) = A_0 \times 10/(A_0 - A_{10}) \quad (2)$$

In the equation, N represents the dilution factor (100); C denotes the protein concentration in g·mL^{-1}; k indicates the oil proportion used for emulsion formation (0.25); L signifies the optical path length (1 cm); A_0 and A_{10} denote the absorbance values of the emulsion at 0 min and 10 min, respectively.

2.4.2.4 Determination of foaming properties

A 15 mL sample solution (10 mg·mL^{-1}) was transferred to a graduated cylinder and homogenized at 12,000 rpm for 2 minutes using a high-speed shear homogenizer (T25, IKA, Germany). Foam volume was recorded immediately (V_1) and after 30 minutes of standing (V_{30}). Foaming capacity (FC) and foam stability (FS) were calculated using the following equations [30].

$$\mathrm{FC}\ (\%) = V_1/15 \times 100 \quad (3)$$

$$\mathrm{FS}\ (\%) = V_{30}/V_1 \times 100 \quad (4)$$

2.4.2.5 Measurement of average particle size and zeta potential

The Mastersizer 2000 particle size analyzer was used to determine the mean particle size and zeta potential of various samples at a concentration of 1 mg·mL^{-1} [31]. The refractive indices for the dispersed and continuous phases were set to 1.33 and 1.46, respectively.

2.4.3 Determination of flavor characteristics

Different samples (1.6 mg·mL^{-1}, w/v) were determined using the electronic tongue system (ASTREE Ⅱ, Alpha MOS, France). The flavor determination includes CTS (salty taste), SCS (bitter taste), AHS (sour taste), NMS (umami taste) and ANS (sweet taste). The sensor is activated in advance with a 0.01 mol·L^{-1} HCl solution. Enter the electronic tongue probe in the alternating sequence of sample–ultrapure water–sample–ultrapure water [32].

2.4.4 Determination of structural characteristics of modified SPI

2.4.4.1 Spectral measurement

Circular dichroism spectra of different SPI samples were measured using a circular dichroism spectrometer (JASCO-1500, JASCO, Japan) to analyze their secondary structures. UV values of different SPI samples were measured between 200–500 nm using a UV spectrophotometer (UV-1900, Japan). Spectra of synchronous and endogenous fluorescence ($\Delta\lambda$ = 15 nm and $\Delta\lambda$ = 60 nm, respectively) were acquired for a range of SPI samples using a fluorescence spectrophotometer (F-7000, Hitachi, Japan).

2.4.4.2 Microstructure determination

Surface topography of different samples was characterized using an atomic force microscope (Multimode 8, Bruker, USA).

2.4.4.3 Determination of surface hydrophobicity

SPI samples were prepared at concentrations ranging from 0.06 to 0.30 mg·mL^{-1}. Each sample was mixed with 20 μL of 1-aniline-8-naphthalenesulfonate (ANS) solution (8 mmol·L^{-1}), incubated in the dark for 3 minutes, and analyzed using a fluorescence spectrophotometer (F-7000, Hitachi, Japan). The excitation wavelength was set at 390 nm, and emission spectra were recorded from 410 to 650 nm [33]. Both excitation and emission slit widths were maintained at 5 nm.

2.4.4.4 Determination of free thiol groups (–SH) and disulfide bond (S–S) content

The sample (10 mg·mL^{-1}) was mixed with 4 mL of

reaction buffer A [0.1 mol·L^{-1} Tris-glycine solution, pH 8.0, containing 1 mol·L^{-1} urea and 0.01mol·L^{-1} ethylene diamine tetraacetic acid (EDTA)] and 125 μL of reaction buffer B [0.1 mol·L^{-1} Tris-glycine solution, pH 8.0, containing 0.01 mol·L^{-1} 5,5'-dithiobis-(2-nitrobenzoic acid) (DTNB)]. The mixture was incubated at 25 °C for 1 hour, after which the sample was read at 412 nm. The sample was mixed with reaction buffer (1 mL of buffer A and 0.02 mL of β-mercaptoethanol) and incubated for 1 hour. The next step involves adding 10 mL of a 12% w/v trichloroacetic acid solution, followed by a reaction at room temperature for 1 hour. Subsequently, the solution was subjected to centrifugation at 8000 rpm for 15 minutes. The precipitate was dissolved in a 12% w/v trichloroacetic acid solution. Following this, the solution was subjected to centrifugation at 10,000 rpm for 10 minutes. The precipitate was dissolved in buffer A, after which the color was developed with 0.01 mol·L^{-1} DTNB buffer B. The total SH content can then be determined by reading the absorption at 412 nm. The free SH, total SH, and disulfide bond contents were calculated according to the following equations:

$$\text{SH content } (\mu\text{mol}\cdot\text{g}^{-1}\text{ protein}) = 73.53 \times OD_{412} \times D/C \quad (5)$$

$$\text{S}-\text{S content} = (\text{total SH content} - \text{free SH content})/2 \quad (6)$$

In the equation, OD_{412} denotes the optical density of the colorimetric solution at a wavelength of 412 nm; D represents the dilution factor; C indicates the sample concentration (mg·mL^{-1}).

2.4.5 Interface property determination

A sample solution with a concentration of 0.4 mg·mL^{-1} was prepared for measuring the interfacial tension. This should be carried out using a droplet tensiometer (Tracker, Teclis Technologies, France). The adsorption of protein molecules on the surface of oil droplets was monitored over a period of three hours. The interfacial tension (π) was calculated using the following equation [34]:

$$\pi = \gamma_o - \gamma_s \quad (7)$$

In the equation, γ_o is representative of the interfacial tension of medium-chain triglycerides (mN·m^{-1}), γ_s is indicative of the interfacial tension of the sample as a function of time (mN·m^{-1}).

The interfacial modulus of different samples at the interface was subsequently determined using amplitude sweep mode. Following a three-hour period during which the samples were adsorbed at the interface, the amplitude was set to 5%, 10%, 20%, 30%, and 40%, with a frequency of 0.1 Hz [34].

2.5 Statistical analysis

All experiments were conducted in triplicate, and the results were presented as means ± standard deviations. Analysis of variance (ANOVA) was used to determine the significant difference among the means at $P < 0.05$, using Duncan's multiple range test with SPSS 27 software (SPSS Inc., Chicago, IL, USA).

3 Results and Discussion

3.1 Optimization of conditions for immobilized PGase-modified SPI

3.1.1 Single-factor experiment

Optimization of reaction conditions was necessary to minimize limited hydrolysis of SPI during deamidation with immobilized PGase, as this process could alter the native structure of SPI and lead to flavor deterioration due to short-peptide formation [35]. The deamidation degree (DD) and hydrolysis degree (DH) of SPI were evaluated under varying temperatures, pH values, and enzyme-to-substrate (E/S) ratios. As illustrated in Figure 1A, DD increased with temperature up to a maximum at 55 °C, after which it declined, while DH remained consistently low. This pattern can be attributed to the increased activity of immobilized PGase below its optimal temperature, which facilitates SPI modification, whereas elevated temperatures have been reported to reduce enzyme activity [36]. Figure 1B demonstrates that the DH of SPI increased gradually with rising pH, although it remained consistently low. In contrast, the DD initially increased before subsequently decreasing. Under acidic conditions (pH 4.0), both SPI solubility and immobilized PGase activity were low. As pH increased, SPI solubility improved, while PGase activity first increased and then declined. Additionally, increasing the amount of immobilized PGase resulted in an initial rise in DD, followed by a decrease (Fig. 1C). This trend can be attributed to substrate competition at excessive enzyme concentrations, which reduces modification efficiency [37]. Throughout these variations, DH exhibited only minor fluctuations and remained low.

3.1.2 Response surface optimization

The results presented in Figure 1 informed the response surface optimization of immobilized PGase-treated SPI, which was conducted using a Box-Behnken design (BBD)

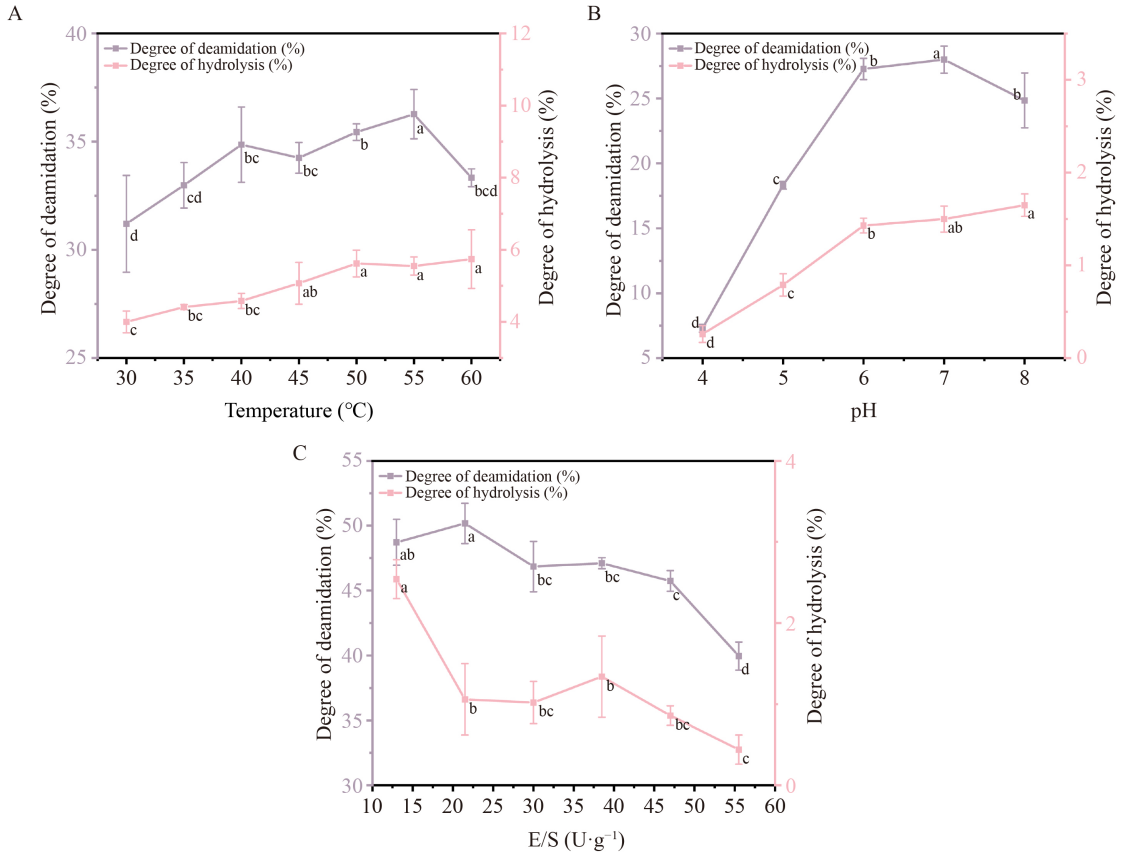

Fig. 1 Effects of temperature (A), pH (B), and E/S ratio (C) on the deamidation and hydrolysis degrees of SPI treated with immobilized PGase.

[38]. Experimental data are provided in Table S1. The subsequent regression equations describe the influence of reaction temperature (A), pH (B), and E/S ratio (C) on the deamidation and hydrolysis degrees of SPI:

$$DD\ (\%) = 47.12 - 0.83A - 0.2512B + 0.7538C - 0.9850AB - 0.64AC + 0.3125BC - 2.00A^2 - 0.2173B^2 - 1.12C^2\ (R^2 = 0.9762,\ CV = 0.54\%)$$

$$DH\ (\%) = 0.9040 - 0.1662A + 0.2287B - 0.06C + 0.115AB - 0.0475AC - 0.0475BC + 0.1680A^2 + 0.463B^2 - 0.0845C^2\ (R^2 = 0.9936,\ CV = 2.32\%)$$

Figure 2A, C, and E illustrate the effects of temperature-pH, temperature-E/S, and pH-E/S interactions on the degree of SPI deamidation, respectively. In comparison, Figure 2B, D, and F present the corresponding effects on the degree of hydrolysis. All three interactions demonstrated favorable trends. Analysis of variance (ANOVA) for the deamidation model (Table S2) demonstrates that the model accurately characterizes the influence of these factors and provides a strong fit. Notably, pH exerted a significant effect ($P < 0.05$), while temperature and E/S ratio exhibited highly significant effects ($P < 0.001$). The lack of fit (0.3864) was not significant ($P > 0.05$), and the low coefficient of variation (0.54%) supports the model's precision and reliability. Similarly, ANOVA for the hydrolysis model (Table S3) confirms its validity, with factor effects aligning with those observed in the deamidation model. The nonsignificant lack of fit (0.3235) and low coefficient of variation (2.32%) further substantiate the model's accuracy and reliability.

In summary, this analysis identified optimal conditions for immobilized PGase treatment to produce soybean protein isolate (SPI) with a high degree of deamidation and a low degree of hydrolysis. The optimal parameters were a reaction temperature of 54.93 °C, a reaction pH of 6.80, and an enzyme-to-substrate ratio of 26.65 $U \cdot g^{-1}$. Under these conditions, the regression model predicted a maximum deamidation degree of 47.19% and a minimum hydrolysis degree of 0.82% for SPI. Experimental validation was conducted, and for practical purposes, the temperature was adjusted to 55 °C while maintaining the other parameters. The resulting SPI demonstrated a deamidation degree of 46.73% and a hydrolysis degree of 0.84%, closely matching the model predictions. These findings confirm the accuracy of the regression model

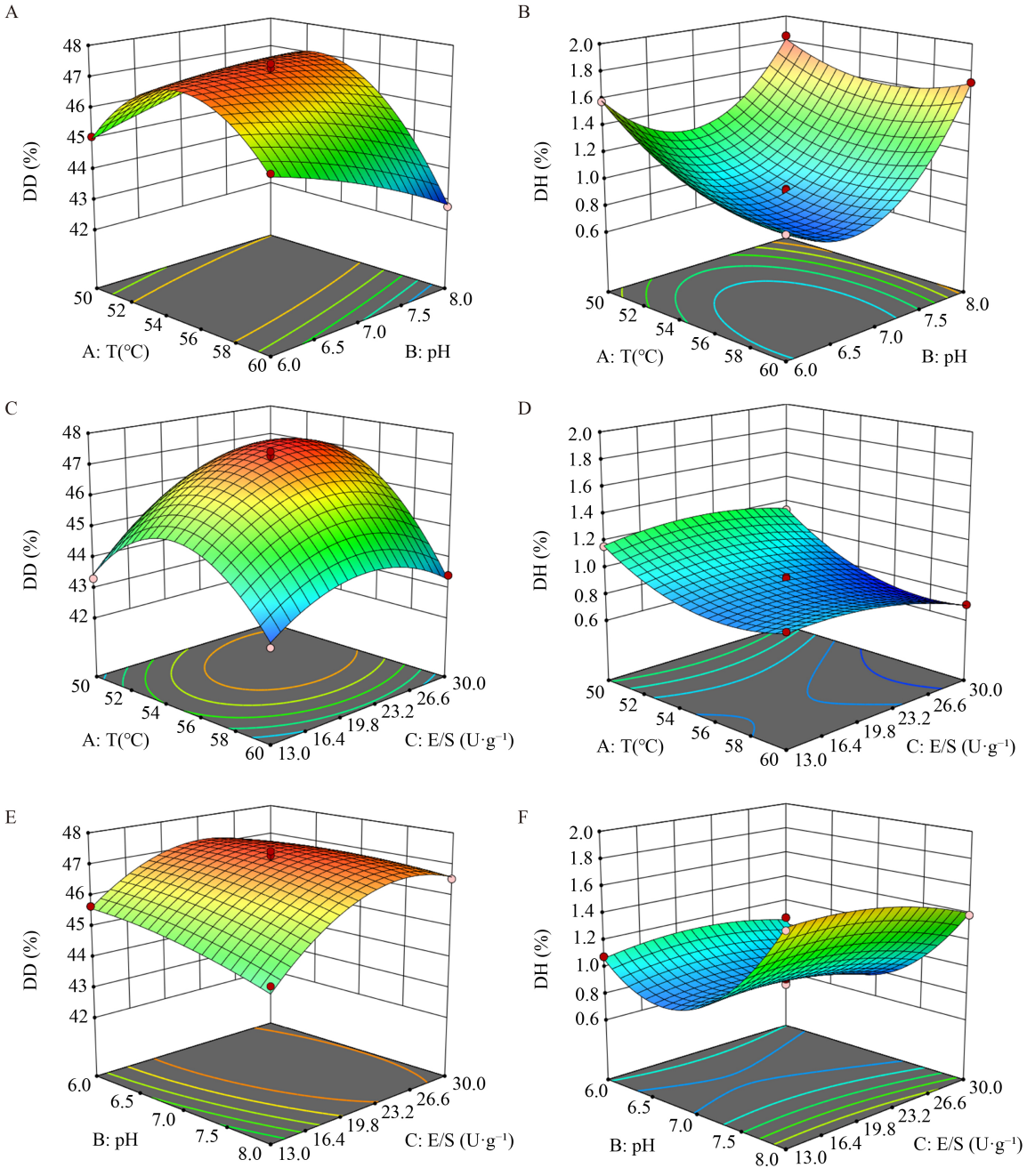

Fig. 2 Effects of interactions among different factors on the deamidation degree (A, C, E) and hydrolysis degree (B, D, F) of SPI.

and indicate that the optimized conditions are applicable in practice.

3.2 Functional properties and aggregation characteristics of modified SPI

3.2.1 Subunit composition and functional characteristics of modified SPI

SDS-PAGE was conducted to examine the subunit composition of SPI before and after deamidation by immobilized PGase (Fig. 3A) [39]. The untreated sample (S0) displayed major bands at 70–100 kDa, 50 kDa, 35–40 kDa, and 15–20 kDa. Following treatment (samples S1–S5), an upward shift in band positions was detected. This shift resulted from deamidation, which converts glutamine amide groups to carboxyl groups, thereby increasing both molecular weight and net negative charge. The increased negative charge likely reduced SDS binding affinity, and the altered charge-to-

mass ratio contributed to the slower migration of certain bands [40,41]. Notably, all major bands from S0 were present in S1–S5, indicating that significant hydrolysis did not occur. Because SPI solubility is positively correlated with emulsifying and foaming properties, solubility changes were also evaluated (Fig. 3B). Solubility increased from 18.83% (S0) to 56.83% (S5) as the degree of deamidation increased. This enhancement is attributed to the introduction of carboxyl groups, which lower the isoelectric point, increase electrostatic repulsion, and promote a more extended protein conformation. As a result, more polar and hydrophilic residues are exposed to the aqueous phase, thereby improving solubility [42].

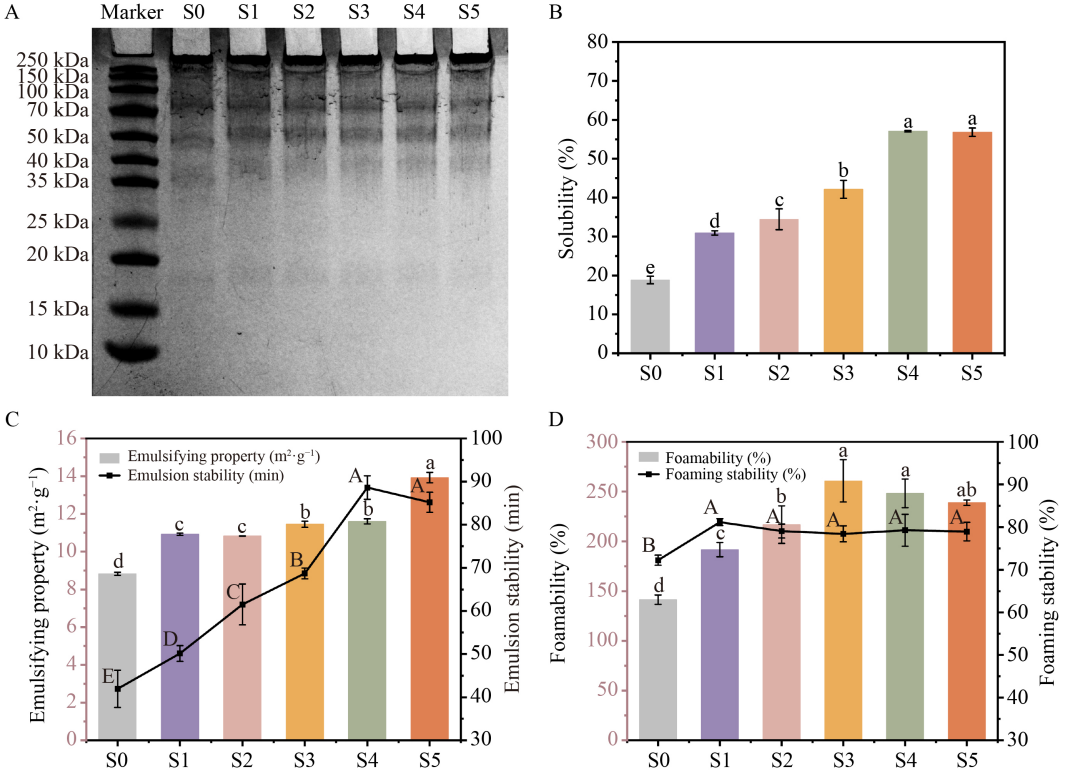

Fig. 3 Subunit composition (A), solubility (B), emulsifying properties (C), and foaming properties (D) of different SPI samples.

Figure 3C demonstrates that S0 exhibited the lowest emulsifying capacity (8.83 $m^2 \cdot g^{-1}$), which increased progressively with higher degrees of deamidation, reaching 13.93 $m^2 \cdot g^{-1}$ for S5. This represents a significant increase of 57.76% ($P < 0.05$). Emulsion stability also improved, rising from 41.94 min for S0 to 88.62 min for S4, after which it remained stable. Similarly, foaming capacity increased with deamidation degree, stabilizing at 260.75% for S4 compared to 141.37% for S0 (Fig. 3D). These trends are attributed to the gradual unfolding of SPI molecules during deamidation, which increases the exposure of hydrophobic and hydrophilic residues. The resulting structural changes enhance the hydrophilic-lipophilic balance, reduce surface tension, and strengthen intermolecular interactions, thereby improving performance at oil–water and gas–liquid interfaces [40,43,44]. As the deamidation degree or reaction time increased further, the modification approached dynamic equilibrium. Under the mild conditions used, the backbone structure of SPI remained intact, underscoring the importance of controlled modification for optimizing functional properties.

3.2.2 Molecular scale of modified SPI

Figure 4A demonstrates that the mean particle size of S1–S4 decreased progressively with increasing deamidation degree and was significantly smaller than that of S0 (177.47 nm). No significant further reduction in particle size was observed for S5 compared to S2–S4. The zeta potential of S0 was −5.45 mV (Fig. 4B), which decreased significantly to −18.39 mV for S4 ($P < 0.05$), while S5 exhibited no additional decline. These changes result from the conversion of amide groups to carboxyl groups during deamidation, which increases the net

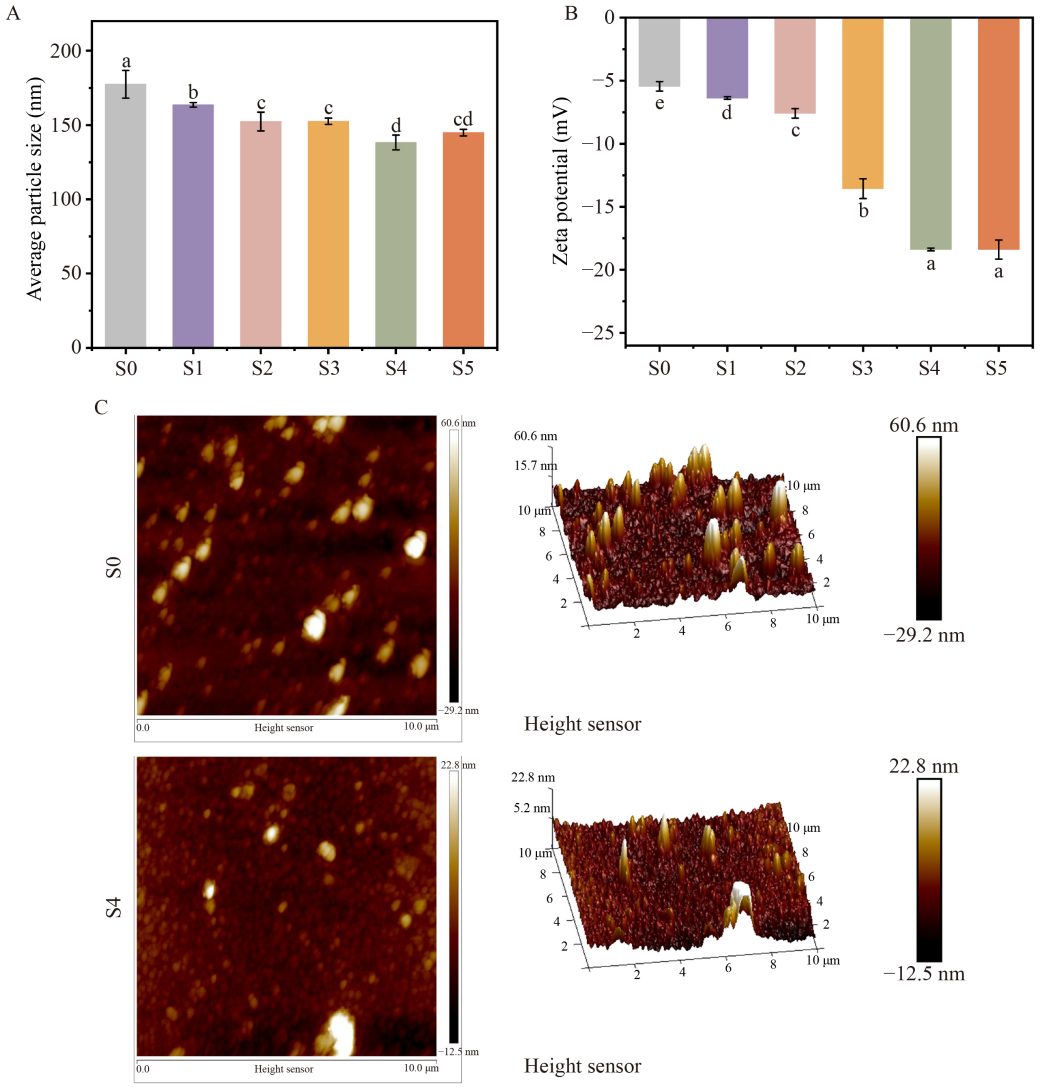

Fig. 4 Average particle size (A), zeta potential (B), and AFM images (C) of different SPI samples.

negative charge on SPI molecules. Enhanced electrostatic repulsion at higher deamidation levels reduces molecular aggregation, resulting in smaller particle sizes, a more extended molecular conformation, and improved dispersion [42]. As a result, the mean particle size decreased, the absolute zeta potential increased, and solution stability improved [45], consistent with the solubility results (Fig. 3B). When enzymatic treatment is prolonged, the deamidation degree approaches a plateau, thereby limiting further substantial changes in structural properties.

The microstructure of SPI before and after deamidation was analyzed using atomic force microscopy (AFM) (Fig. 4C) [46]. In the AFM images, protein aggregates appeared as white dots, where higher aggregate density indicated reduced molecular dispersion [47]. Compared with S0, which displayed numerous large protein clusters, S4 exhibited a markedly lower number of aggregates. This reduction can be attributed to increased electrostatic repulsion between molecules, which enhances the dispersion of SPI in water [42]. These findings are consistent with the solubility (Fig. 3B) and particle size measurements (Fig. 4A).

3.2.3 Flavor characteristics of modified SPI

The flavor profiles of various SPI samples were evaluated using an electronic tongue (Fig. 5A). Compared with S0, S4 showed a significantly higher saltiness score, attributed to an increased number of carboxyl groups introduced by deamidation. This modification enhances ionic strength and, consequently, saltiness perception [48]. As shown in Figure S2, as the deamidation reaction proceeded, the content of carboxyl

groups in the SPI molecule gradually increased. The substantial increase in umami score observed in S4 is likely due to elevated glutamic acid content [25]. Additionally, deamidation causes the SPI structure to unfold, exposing more amino acid residues capable of binding sour taste receptors, resulting in a higher sourness score. The bitterness score of S4 was significantly lower than that of S0, potentially because structural unfolding alters secondary and tertiary folding, thereby reducing the capacity of hydrophobic clusters to retain undesirable flavors [49]. Principal component analysis (Fig. 5B) confirmed the distinct flavor profiles between S0 and S4, supporting these interpretations. Collectively, these findings indicate that deamidation can enhance desirable flavors, such as saltiness and umami, while suppressing undesirable flavors, such as bitterness. This highlights the potential of deamidation to expand SPI applications within the food industry.

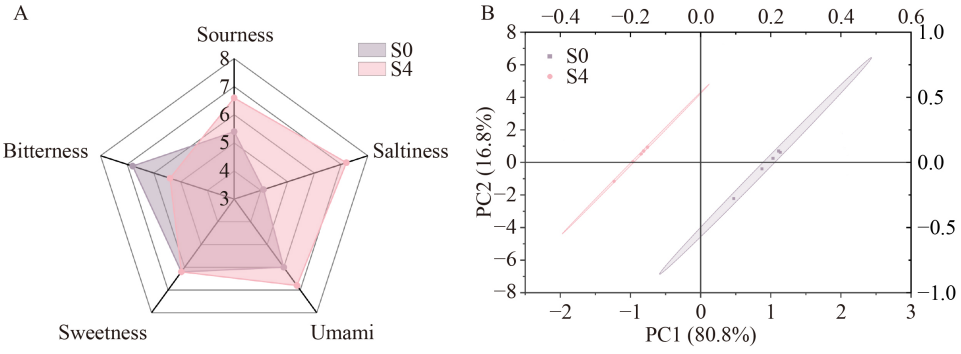

Fig. 5 Flavor characteristics of different SPI samples.

3.2.4 Secondary structure and surface hydrophobicity of modified SPI

Figure 6A presents the secondary structure proportions of various SPI samples. In the S0 sample, the relative contents of α−helix, β−sheet, and random coils were 22.05%, 21.80%, and 40.95%, respectively. As the degree of deamidation increased, the proportions of α−helix and β−sheet decreased significantly, whereas the content of random coils increased markedly. In the S4 sample, α−helix and β−sheet contents declined to 17.20% and 18.50%, respectively, while random coils increased to 46.60%. No significant difference was observed between S5 and S4. These structural changes are attributed to the conversion of amide groups to carboxyl groups during deamidation, which increases negative charges and enhances electrostatic repulsion, while weakening hydrogen bonds and hydrophobic interactions. As a result, α−helices unwind, and β−sheets unfold [50], leading to a gradual transition from a compact, ordered conformation to a more extended and disordered state that promotes random coil formation [45].

Figure 6B presents the FTIR spectra of various SPI samples. In the S0 sample, characteristic peaks at 3308.89 cm^{-1} and 1396.19 cm^{-1} correspond to O–H stretching and –COO– vibrations, respectively [51]. After deamidation, both peaks shifted to higher wavenumbers. This shift is attributed to the more extended molecular structure of SPI, in which increased electrostatic repulsion disrupts the hydrogen-bond network, reducing hydrogen bonding and consequently expanding the bond force constant and vibration frequency [52].

The contents of free sulfhydryl (–SH) and disulfide (S–S) bonds, which directly influence protein structure and interfacial properties, were quantified (Fig. 6C) [53]. With increasing deamidation, the free –SH content increased from 4.09 $\mu mol \cdot g^{-1}$ (S0) to 5.79 $\mu mol \cdot g^{-1}$ (S5), while the S–S content decreased from 64.96 $\mu mol \cdot g^{-1}$ to 46.33 $\mu mol \cdot g^{-1}$. This trend is attributed to enhanced molecular flexibility and to a more disordered structure resulting from deamidation, which weakens hydrogen bonds and hydrophobic interactions and promotes S–S bond cleavage [54]. These results are consistent with the observed reduction in α-helix and β-sheet content shown in Figure 6A. Surface hydrophobicity (H_0), which reflects the exposure of hydrophobic groups [55], increased from 1297.23 (S0) to 2238.63 (S5) as deamidation progressed (Fig. 6D). This increase results from the progressive unfolding of SPI molecules, which exposes previously inaccessible hydrophobic regions [15]. Collectively, these findings indicate that once the degree of deamidation plateaus, additional enzymatic treatment does not induce significant structural changes in SPI.

3.2.5 Tertiary structure of modified SPI

Ultraviolet (UV) spectroscopy is a valuable tool for investigating the tertiary structure of proteins, as aromatic

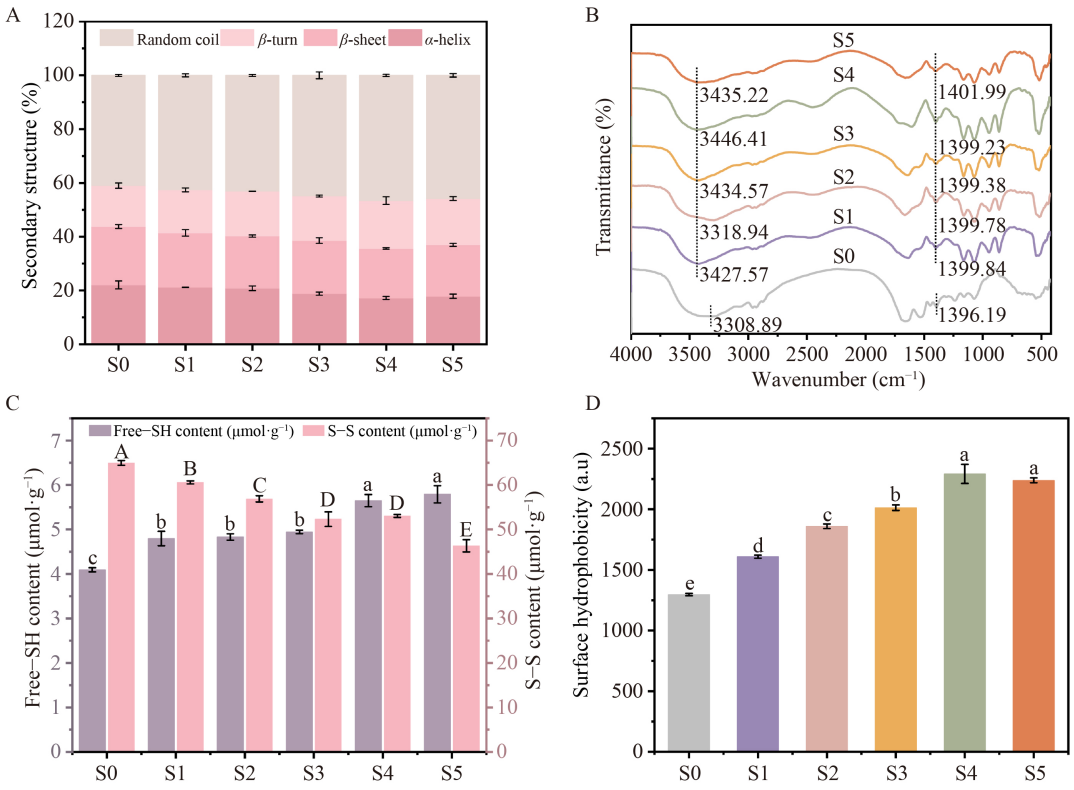

Fig. 6 Secondary structure proportions (A), FTIR spectra (B), free sulfhydryl-disulfide bond content (C), and surface hydrophobicity (D) of different SPI samples.

amino acids such as tyrosine, tryptophan, and phenylalanine display characteristic UV absorption peaks [56]. Fig. 7A presents the UV spectra of various SPI samples. In comparison to S0, the characteristic absorption peaks of S1–S5 exhibited a progressive red shift. This red shift is attributed to deamidation, a process reported to increase molecular flexibility, weaken hydrogen bonds, and alter the secondary structure of SPI. These structural modifications collectively change the microenvironment surrounding aromatic amino acid residues in SPI molecules [57–59]. Previous studies have demonstrated a clear correlation between the red shift of UV absorption peaks and increased protein extensibility, which is consistent with the present findings [59].

Endogenous fluorescence spectroscopy is widely employed to analyze the tertiary structure of protein [60]. As illustrated in Figure 7B, S0 showed the highest fluorescence intensity at 339 nm. In deamidated samples S1–S4, the maximum peaks occurred at similar wavelengths, with fluorescence intensity increasing alongside the degree of deamidation. These findings indicate that moderate deamidation promotes structural expansion and flexibility in SPI, thereby increasing the exposure of hydrophobic amino acid residues and, consequently, the fluorescence intensity. Synchronous fluorescence spectroscopy provides insight into the microenvironment surrounding chromophores in SPI [61]. At wavelength intervals of 15 nm (Fig. 7C) and 60 nm (Fig. 7D), the signals correspond to tyrosine and tryptophan residues, respectively [62]. The greater intensity observed at 60 nm suggests that tryptophan contributes more substantially to SPI's overall fluorescence [63]. Furthermore, fluorescence intensities at both time points increased with the degree of deamidation, consistent with the endogenous fluorescence results (Fig. 7B).

3.2.6 Interfacial properties of modified SPI

Figure 8A demonstrates that the interfacial tension at the oil–water interface increased linearly with $t^{1/2}$ during the initial adsorption stage, indicating that protein adsorption was diffusion-controlled and proceeded rapidly. The adsorption curve for S4 exhibited a steeper slope than that of S0, reflecting a faster diffusion and adsorption rate [34]. In the subsequent stage, the interfacial tension stabilized for both S0 (approximately 19 mN·m^{-1}) and S4 (approximately 17 mN·m^{-1}) by 10,800 s. Throughout the adsorption process, S4 showed a greater overall reduction in interfacial tension than S0 (Fig. 8B). This difference is

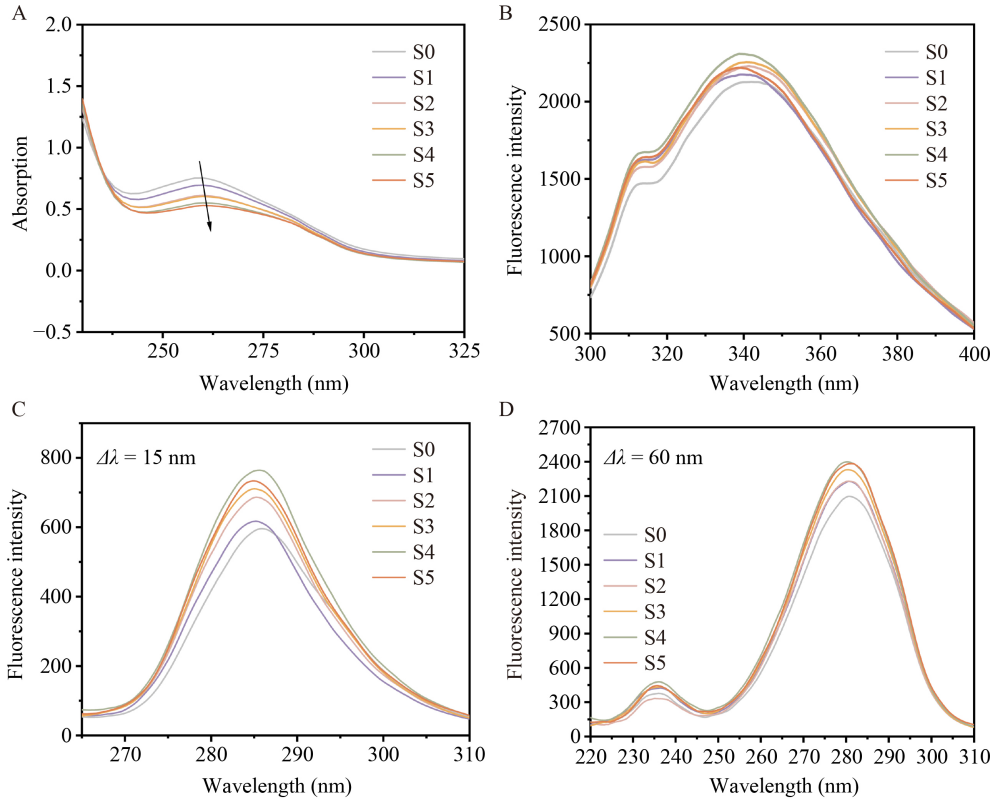

Fig. 7 UV spectra (A), autofluorescence spectra (B), and synchronous fluorescence spectra (C–D) of different SPI samples.

attributed to the more flexible and extended conformation of deamidated SPI, which facilitates diffusion to the interface, followed by unfolding and rearrangement [64]. These findings are consistent with the previously discussed emulsification performance (Fig. 3C).

Amplitude sweeps were conducted to further investigate interfacial properties at the oil–water interface. In Lissajous plots of interfacial tension versus deformation amplitude, elastic films generally yield linear patterns, while viscous films display circular patterns. Symmetric ellipses indicate linear viscoelastic responses, whereas asymmetric ellipses reflect nonlinear behavior [64,65]. As illustrated in Figure 8C, the Lissajous plots for S0 and S4 showed nearly symmetric ellipses at low amplitudes (5% and 10%), corresponding to linear viscoelasticity. With increasing amplitude to approximately 40%, the plots became more asymmetric, indicating structural breakdown and a directional, nonlinear viscoelastic response at high strain [34,65]. The plot for S4 was slightly more tilted toward the horizontal axis compared to S0, suggesting that S4 adsorbed, unfolded, and rearranged more efficiently at the interface, resulting in a dense, flexible film with enhanced stability [34]. This behavior is attributed to deamidation, which increases amphiphilicity by exposing additional hydrophilic and hydrophobic residues, consistent with the interfacial adsorption results (Fig. 8A, B).

The microstructure of the SPI-stabilized oil–water interface was characterized using cryo-scanning electron microscopy (Fig. S3) [66]. Untreated SPI exhibited a rough interface with adhered particles of varying sizes, attributed to molecular aggregation and reduced flexibility that impede effective adsorption and stabilization [34]. In contrast, deamidated SPI produced a more uniform interfacial film. This improvement is attributed to the extended and flexible conformation of deamidated molecules, which enhances adsorption, unfolding, and rearrangement at the interface, resulting in a dense, flexible film that more effectively resists emulsion coalescence and demulsification [34]. These findings align with the previously discussed emulsification performance (Fig. 3C).

Based on the above analysis, the mechanism of SPI modified by immobilized PGase can be summarized as follows (Fig. 9). First, the easy separation of immobilized PGase from the reaction system avoids the detrimental effects of conventional high-temperature enzyme inactivation on SPI. Second, the mild, controllable deamidation converts amide groups in SPI into carboxyl groups. This increase in negative charge enhances intermolecular electrostatic repulsion, weakens hydrogen bonding and hydrophobic interactions, and results in a

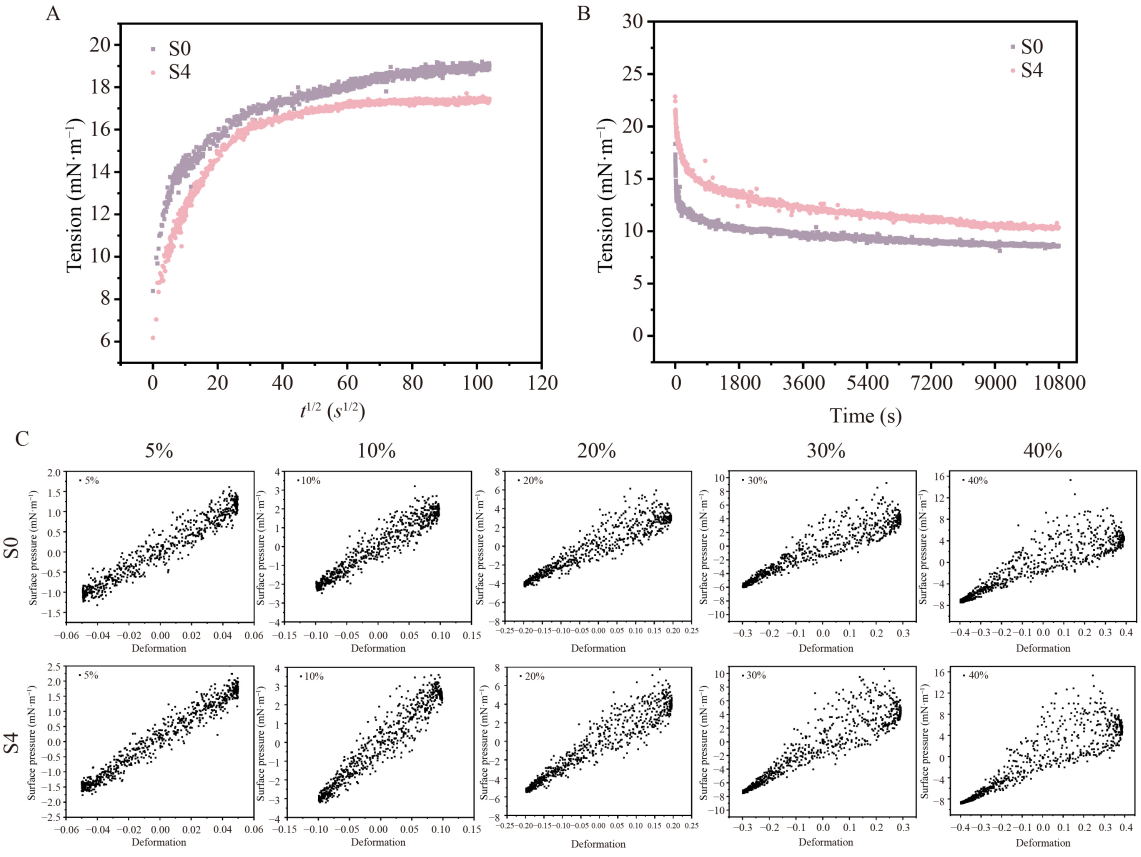

Fig. 8 Interfacial adsorption (A–B), and Lissajous figures (C) of different SPI samples.

more extended and flexible molecular conformation, thereby improving the solubility and other functional properties of SPI. Furthermore, the modified SPI exhibits altered secondary and tertiary structures, including reduced disulfide bond content and increased surface hydrophobicity. These changes enhance both hydrophilicity and lipophilicity, promoting stability at the oil–water interface.

4 Conclusion

In summary, this study achieved mild and controllable deamidation of SPI using immobilized PGase, elucidating the structure-unction relationship between deamidation degree and the molecular structure and functional properties of SPI. Reaction conditions—including temperature, pH, and enzyme-to-substrate ratio—were optimized. Under the conditions of 54.95 °C, pH 6.80, and an E/S ratio of 26.65 $U \cdot g^{-1}$, a high deamidation degree was attained while hydrolysis remained low. The mild, controlled deamidation by immobilized PGase improved the functional properties of SPI, which first increased and then stabilized as the degree of deamidation increased. Analysis of structural changes indicated that moderately deamidated SPI adopts a more extended and flexible conformation, with a smaller particle size, higher surface hydrophobicity, and lower surface tension, facilitating diffusion to interfaces where proteins rapidly adsorb, unfold, and reorganize. These combined effects enhance the functional performance of modified SPI. Additionally, the modified SPI showed improved flavor characteristics, with increased saltiness and umami perception and reduced bitterness. At higher deamidation levels, the enzymatic modification maintained SPI backbone integrity, avoided excessive hydrolysis, and ensured structural and functional stability. Thus, immobilized PGase-mediated deamidation proves effective and offers theoretical insight for broadening the application of SPI in the food industry. Further studies could examine the nutritional profile of deamidated plant proteins and assess their practical applications in the food industry, particularly by utilizing their improved functional properties in products such as ice cream, cakes, and other formulated foods.

Supporting Information Supporting Information is available in the online version of this article at https://doi.org/10.2738/ENGB.2026.0003 and is accessible for authorized users.

Data availability The datasets used and/or analyzed during the current

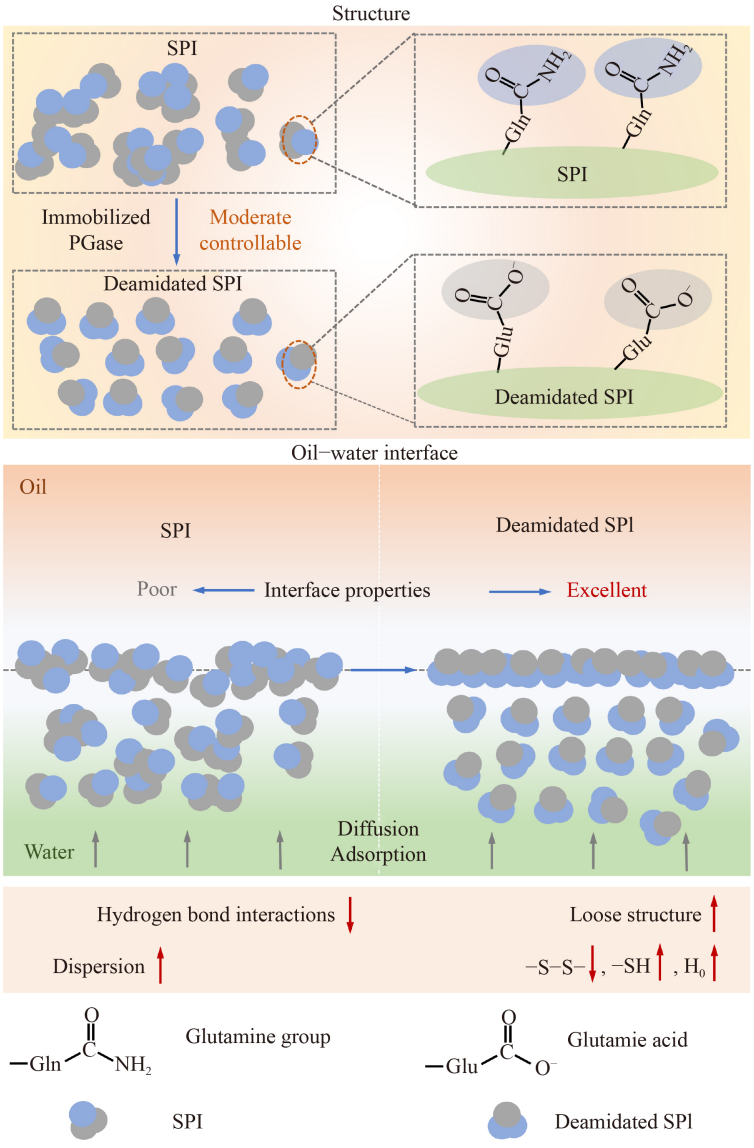

Fig. 9 Mechanism diagram of mild and controllable deamidation modification of SPI.

study are available from the corresponding author upon reasonable request.

Acknowledgments This work was supported by the Central Public-interest Scientific Institution Basal Research Fund (No. Y2026QC29); the National Key Research and Development Program of China (2024YFD1600105); the National Natural Science Foundation of China (Grant No. 32302149); the Central Public-interest Scientific Institution Basal Research Fund in CAAS (No. 1610172023005); the Knowledge Innovation Program of the Wuhan-Shuguang Project (Oil Crops Research Institute of the Chinese Academy of Agricultural Sciences 2023020201020397); the Key Research and Development Project of Shanxi Province - Research and Demonstration on Key Technologies for Improving Quality and Efficiency of Plant-Based Protein Resources and Black Agricultural Products (2022ZDYF123); the Taishan Industrial Experts Program. The authors used DeepSeek (online version) as a language-editing tool to improve grammar, clarity, and readability. The AI tool was not used for data analysis, data generation, image processing, or scientific content creation. All outputs were carefully reviewed and verified by the authors, who take full responsibility for the final content.

Competing interests The authors declare no conflicts of interest.

References

1. Sarathy S P, Ravikumar H, Nanjan P, et al. Plant-based protein: a multi-nutritional sustainable alternative to animal foods and their structure, functions, and relationship: A review. International Journal of Biological Macromolecules, 2025, 321(Pt 3): 146465
2. Li M Z, Zou L, Zhang L Z, et al. Plant-based proteins: advances in their sources, digestive profiles *in vitro* and potential health benefits. Critical Reviews in Food Science and Nutrition, 2025, 65(10): 1929−1949
3. Eze F N, Muangrat R, Jirarattanarangsri W, et al. Sesame seed

meal as a sustainable source of high-quality plant-based proteins: delineating recent advances in the preparation, composition, techno-functionalities, and food industry applications. Comprehensive Reviews in Food Science and Food Safety, 2025, 24(3): e70188

4. Cavaliere C, Montone A M I, Aita S E, et al. Production and characterization of medium-sized and short antioxidant peptides from soy flour-simulated gastrointestinal hydrolysate. Antioxidants, 2021, 10(5): 734
5. Hammer L, Moretti D, Bétrix C A, et al. *In vitro* DIAAS of Swiss soybean cultivars using the INFOGEST model: increase in protein quality from soybean to soymilk and tofu. Food Research International, 2024, 178: 113947
6. Peng Z Q, Liu K L, Liao N. Effect of TGase crosslinking on the structure, emulsification, and gelling properties of soy isolate proteins. Foods, 2025, 14(12): 2130
7. Fan X, Zhang Y Y, Sun Y, et al. Deterioration mechanism for the solubility of skimmed egg yolk powder: powder characteristics, rehydration capability and protein structure. Food Chemistry, 2025, 493(Pt 1): 145675
8. Gao K, Rao J J, Chen B C. Plant protein solubility: A challenge or insurmountable obstacle. Advances in Colloid and Interface Science, 2024, 324: 103074
9. An D, Li L. Synergistic treatment of pH and ultrasound promotes the formation of insoluble soy protein hydrolysate nanofibrils. Food Chemistry, 2025, 470: 142659
10. Geng M J, Feng X M, Wu X X, et al. Characterization and utilization of soy protein isolate-(-)-epigallocatechin gallate-maltose ternary conjugate as an emulsifier for nanoemulsions: enhanced physicochemical stability of the β-carotene nanoemulsion. Food Chemistry, 2023, 417: 135842
11. Dent T, Campanella O, Maleky F. Enzymatic hydrolysis of soy and chickpea protein with Alcalase and Flavourzyme and formation of hydrogen bond mediated insoluble aggregates. Current Research in Food Science, 2023, 6: 100487
12. Santana I, Felix M, Bengoechea C. Properties of biopolymer blends based on *Rugulopteryx okamurae* and hydrophobic polycaprolactone (PCL) and hydrophilic acylated soy protein isolated (SPIa). Environmental Science and Pollution Research, 2024, 31(25): 36615−36625
13. Zhu J, Yu L, Stockmann R, et al. Thermal treatment of alkali lignin to eliminate its inhibition of pancreatic proteases *in vitro*. Food Chemistry, 2024, 442: 138412
14. Yang J H, Gao Z Q, Ren X H, et al. DeepDigest: prediction of protein proteolytic digestion with deep learning. Analytical Chemistry, 2021, 93(15): 6094−6103
15. Fu W Y, Chen X, Cheng H, et al. Tailoring protein intrinsic charge by enzymatic deamidation for solubilizing chicken breast myofibrillar protein in water. Food Chemistry, 2022, 385: 132512
16. Zhang L, You Y Y, Zhang K, et al. Improving solubility of rice protein powder by modifying its physicochemical properties by ultrasound-assisted protein-glutaminase. Food Chemistry, 2025, 464: 141627
17. Vidotto D C, Galvão A M M T, Tavares G M, et al. Does protein deamidation enhance rice protein concentrate's ability to produce and stabilize high internal phase emulsions?. Food Research International, 2024, 179: 114012
18. Chen X, Fu W Y, Luo Y C, et al. Protein deamidation to produce processable ingredients and engineered colloids for emerging food applications. Comprehensive Reviews in Food Science and Food Safety, 2021, 20(4): 3788−3817
19. Kamani M H, Semwal J, Mousavi Khaneghah A. Functional modification of grain proteins by dual approaches: current progress, challenges, and future perspectives. Colloids and Surfaces B: Biointerfaces, 2022, 211: 112306
20. Martínez Y B, Ferreira F V, Musumeci M A. l-Glutamine-, peptidyl- and protein-glutaminases: structural features and applications in the food industry. World Journal of Microbiology and Biotechnology, 2022, 38(11): 204
21. Sewa A S, Besser H A, Mathews I I, et al. Structural and mechanistic analysis of Ca^{2+}-dependent regulation of transglutaminase 2 activity using a Ca^{2+}-bound intermediate state. Proceedings of the National Academy of Sciences of the United States of America, 2024, 121(28): e2407066121
22. Zhang Z, Li Y X, Zheng L H, et al. A novel method for high level production of protein glutaminase by sfGFP tag in *Bacillus subtilis*. International Journal of Biological Macromolecules, 2024, 262(Pt 2): 130092
23. Teng M F, Zhang J, Zhou J W, et al. Regulation of proenzyme activation and metabolic engineering for protein-glutaminase production in *Bacillus subtilis*. Metabolic Engineering, 2025, 91: 336−346
24. Liu X, Wang C, Zhang X W, et al. Application prospect of protein-glutaminase in the development of plant-based protein foods. Foods, 2022, 11(3): 440
25. Leng W J, Li Y, Liang X, et al. Thermo-reversible gelation and enhanced umami perception of myofibrillar proteins induced by protein-glutaminase-mediated deamidation. Food Chemistry, 2025, 471: 142802
26. Zhou C C, Deng J Y, Tay J H, et al. Multifunctional material building blocks from plant pollen. Annual Review of Chemical and Biomolecular Engineering, 2024, 15(1): 1−24
27. Walkling-Ribeiro M, Jacob T, Ahrné L. Impact of pulsed electric field intensity on the cream separation efficiency from bovine milk and physico-chemical properties of the cream. Food Research International, 2024, 180: 114074
28. Maria Tottoli E, Chiesa E, Ceccarelli G, et al. BioFiber: an advanced fibrous textured dressing to manage exudate in severe wounds. International Journal of Pharmaceutics, 2022, 625: 122073
29. Zheng X T, Cheng T F, Liu S B, et al. Ultrasonic combined pH shifting strategy for improving the stability of emulsion stabilized by yeast proteins: focused on solubility, protein structure, interface properties. International Journal of Biological Macromolecules, 2025, 293: 139396
30. Zhang S Y, Hao J L, Xie Q G, et al. pH-induced physiochemical and structural changes of milk proteins mixtures and its effect on foaming behavior. International Journal of Biological

Macromolecules, 2024, 254(Pt 2): 127838
31. Othmeni I, Blecker C, Karoui R. pH-dependent emulsifying properties of pea protein isolate: investigation of the structure - function relationship. International Journal of Biological Macromolecules, 2025, 290: 139105
32. Wang X Y, Dai X X, Li J, et al. Preparation of hollow salt particles based on multiple salt reduction strategies for enhanced saltiness perception. Food Hydrocolloids, 2026, 170: 111646
33. Rajasekaran B, Singh A, Ponnusamy A, et al. Ultrasound treated fish myofibrillar protein: physicochemical properties and its stabilizing effect on shrimp oil-in-water emulsion. Ultrasonics Sonochemistry, 2023, 98: 106513
34. Yang J, Duan Y Q, Zhang H H, et al. Ultrasound coupled with weak alkali cycling-induced exchange of free sulfhydryl-disulfide bond for remodeling interfacial flexibility of flaxseed protein isolates. Food Hydrocolloids, 2023, 140: 108597
35. Kunarayakul S, Thaiphanit S, Anprung P, et al. Optimization of coconut protein deamidation using protein-glutaminase and its effect on solubility, emulsification, and foaming properties of the proteins. Food Hydrocolloids, 2018, 79: 197−207
36. Wu J H, Wang Z J, Zeng M M, et al. Comprehensive understanding of laboratory evolution for food enzymes: from design to screening innovations. Journal of Agricultural and Food Chemistry, 2024, 72(45): 24928−24943
37. Lortie R, André G. On the use of apparent kinetic parameters for immobilized enzyme with noncompetitive substrate inhibition. Enzyme and Microbial Technology, 1991, 13(12): 960−963
38. Sahin B, Ozbey-Unal B, Dizge N, et al. Optimization of immobilized urease enzyme on porous polymer for enhancing the stability, reusability and enzymatic kinetics using response surface methodology. Colloids and Surfaces B: Biointerfaces, 2024, 240: 113986
39. Duan C C, Wu C, Zhang Y, et al. Protein structure modification and allergenic properties of soybean protein isolate in combination with (-)-epigallocatechin gallate and exopolysaccharides. International Journal of Biological Macromolecules, 2025, 314: 144351
40. Xiong T, Xiong W F, Ge M T, et al. Effect of high intensity ultrasound on structure and foaming properties of pea protein isolate. Food Research International, 2018, 109: 260−267
41. Yu Y T, Gong W, Liu H, et al. Insights into the enhancement mechanism of rheological properties of dough induced by wheat flour maturation: the view from gluten proteins aggregation. International Journal of Biological Macromolecules, 2024, 282(Pt 2): 136942
42. Li Z Y, Wang K N, Ding Y N, et al. Pickering emulsion stabilized by protein-glutaminase modified soybean isolated proteins as a new delivery system. Food Chemistry, 2025, 483: 144334
43. Zhu R, Zhang J, Meng Z. Synergistic stabilization of oil-in-water emulsion gels by pea protein isolate and cellulose nanocrystals: effects of pH and application to 3D printing. Food Chemistry, 2025, 468: 142480
44. Lian Z T, Yang S, Cheng L, et al. Emulsifying properties and oil–water interface properties of succinylated soy protein isolate: affected by conformational flexibility of the interfacial protein. Food Hydrocolloids, 2023, 136: 108224
45. Zhang Q, Ouyang K F, Huang F, et al. Evaluating the effects of protein-glutaminase treatment on the structural and functional properties of pumpkin (*Cucurbita moschata*) seed protein. International Journal of Biological Macromolecules, 2025, 309(Pt 2): 142989
46. Kodera N, Noshiro D, Dora S K, et al. Structural and dynamics analysis of intrinsically disordered proteins by high-speed atomic force microscopy. Nature Nanotechnology, 2021, 16(2): 181−189
47. Li Y H, Zhang Z L, Ren W B, et al. Inhibition effect of ultrasound on the formation of lysinoalanine in rapeseed protein isolates during pH shift treatment. Journal of Agricultural and Food Chemistry, 2021, 69(30): 8536−8545
48. Qi J M, Qin Y M, Wang W Z, et al. Saltiness enhancement of soy peptides by modulating amiloride-insensitive salt-responsive cells and interacting with cell membranes. Journal of Agricultural and Food Chemistry, 2025, 73(9): 5423−5435
49. Zhao Q, Li Z X, Zhang K E, et al. Revealing the off-flavors in hydro-distilled essential oils of sweet orange (*Citrus sinensis*) by flavoromics strategy and computational simulation. Food Chemistry, 2025, 465(Pt 1): 141990
50. Frempong K E B, He G Q, Kuang M, et al. Improvement of amphipathic properties with molecular structure unfolding and activation of cottonseed protein as ultra stable and safe emulsifier by deamidation. International Journal of Biological Macromolecules, 2023, 247: 125802
51. Rajapaksha R A N D, Leelamanie D A L, Mori Y. Heat-induced changes in water repellency of litter ash: role of organic functional groups as determined by FTIR spectroscopy. Science of the Total Environment, 2025, 981: 179594
52. Heller J, Tang W K, Cunningham E M, et al. Getting ready for the hydrogen evolution reaction: the infrared spectrum of hydrated aluminum hydride-hydroxide $HAlOH^{+}(H_2O)_{n\text{-}1}$, n=9-14. Angewandte Chemie International Edition, 2021, 60(31): 16858−16863
53. Roy T, Pawar A, Singh A, et al. A comprehensive review on rice proteins: composition, structural modification, functional and industrial food applications. Critical Reviews in Food Science and Nutrition, 2025, 65(34): 8842−8859
54. Tanriver G, Monard G, Catak S. Impact of deamidation on the structure and function of antiapoptotic Bcl-x_L. Journal of Chemical Information and Modeling, 2022, 62(1): 102−115
55. De la Cruz-Torres L F, Rodríguez-Celestino V, Centeno-Leija S, et al. Development of a rapid, high-sensitivity, low-cost fluorescence method for protein surface hydrophobicity determination using a Nanodrop fluorospectrometer. Food Chemistry, 2022, 396: 133681
56. Lian Z T, Yang S, Liu X Y, et al. Soy glycinin-carboxymethyl cellulose “chain bead-like” nanocomplexes: focus on formation mechanism, functional characteristics and stability properties. Food Hydrocolloids, 2025, 159: 110617
57. Li Z Y, Wang K N, Li M Y, et al. Enzymatic deamidation soy protein isolate stabilized high internal phase emulsion as a new fat

substitute in meat patties. Food Research International, 2025, 218: 116935

58. Rozas I, Alkorta I, Elguero J. Modeling protein−RNA interactions: an electron-density study of the formamide and formic acid complexes with RNA bases. The Journal of Physical Chemistry B, 2004, 108(10): 3335−3341
59. Heidary A, Soltanizadeh N. The effects of high-pressure homogenization on physicochemical and functional properties of gelatin. Food and Bioprocess Technology, 2024, 17(1): 100−122
60. Dubey S, Mishra N, Goswami N, et al. Multimodal approach to characterize the tetrameric form of human PML-RBCC domain and ATO-mediated conformational changes. International Journal of Biological Macromolecules, 2022, 223(Pt A): 468–478
61. Zhang H X, Chen G J, Liu M, et al. Effects of multi-frequency ultrasound on physicochemical properties, structural characteristics of gluten protein and the quality of noodle. Ultrasonics Sonochemistry, 2020, 67: 105135
62. Osman M M, El-Shaheny R, Ibrahim F A. Perception of the interaction behavior between pepsin and the antimicrobial drug secnidazole with combined experimental spectroscopy and computer-aided techniques. Spectrochimica Acta Part A: Molecular and Biomolecular Spectroscopy, 2023, 291: 122336
63. Chen S W, Tao C Y, Huang Y W, et al. Modulation of protein glutaminase α-helix and disulfide bonds in a sunflower pollen microgel microenvironment: a strategy to enhance enzyme activity and stability. Food Chemistry, 2025, 480: 143561
64. Zhou J S, Yang J, Shao J Q, et al. Composition, structure, and interfacial rheological properties of walnut glutelin. Applied Rheology, 2025, 35(1): 20250047
65. Yang J, Li D P, Ashokkumar M, et al. Flaxseed protein isolates-stabilized oil-water interface: role of globulin and albumin. Food Hydrocolloids, 2026, 172: 111913
66. Guo F X, Mao Y M, Chen Y J, et al. Medium internal phase emulsions stabilized by soy protein isolates: protein solubility effect and stabilization mechanism. Foods, 2025, 14(12): 2028